Dynamics of gas bubbles in monolayers

Bruno Berge,* Adam J. Simon, and Albert Libchaber
The James Franck and Enrico Fermi Institutes, 5640 South Ellis Avenue, Chicago, Illinois 60637
(Received 8 January 1990)

We present a study of the temporal evolution of a two-dimensional bubble pattern in the liquid-gas coexistence region of monolayers. Using fluorescence microscopy of pentadecanoic acid or dipalmitoyl phosphotidylcholine on the surface of water, we study the coarsening of the pattern for several days. Two different regimes appear, depending on the percentage of gas phase observed on the surface. At high gas coverage ($\sim 75\%$), we observe "polygonal" gas bubbles separated by thin liquid lines like a two-dimensional soap froth. We confirm the results of Glazier and co-workers [J. A. Glazier, S. P. Gross, and J. Stavans, Phys. Rev. A **36**, 306 (1987); J. Stavans and J. A. Glazier, Phys. Rev. Lett. **62**, 1318 (1989)] on the nature of the asymptotic scaling states, but find a growth exponent $\alpha \approx 1.0$ for the time evolution of the mean area. At intermediate gas coverage ($\sim 50\%$), we observe weakly interacting "circular" gas bubbles, which grow at a slower rate with an exponent $\alpha \approx 0.6$. This state does not reach a scaling regime: The probability distribution for bubble areas broadens continuously and develops a power law at late-stage. The pattern itself evolves toward a critical object. Also, secondary nucleation of tiny liquid droplets in the gas bubbles is observed. The relevance of long-range dipolar interactions is discussed.

I. INTRODUCTION

Recently the dynamics of phase growth in two dimensions has led to interesting forms, revealing surprising phenomena such as fractal objects,[1] spiral crystals,[2] etc. The growths and forms in nonequilibrium systems like soap froths,[3] breath figures,[4] or magnetic bubbles[5] also lead to interesting collective patterns.[6]

In this paper we present an experimental study of the long-term evolution of gas bubbles in lipid monolayers. The film is maintained at fixed area and temperature in the liquid-gas coexistence region. The system is ideally of the "conserved-order-parameter" type,[7] meaning that the overall percentage of liquid and gas remains constant. The initial configuration is obtained by spreading the molecules on the surface of water with a solvent which then evaporates. One observes a set of small gas bubbles in a liquid background. In time, the pattern coarsens to decrease its interfacial energy, at a rate which is limited by molecular diffusion. This occurs by contracting small bubbles and expanding large ones, without bubble fusion. A study of the asymptotic behavior of this (almost) perfect two-dimensional system is the aim of our paper.

These experiments evolved from the results of Glazier *et al.*[8-10] on soap froths in quasi-two-dimensional geometries. They showed that the froth reaches a scaling state, where the topology is stable, and the mean bubble size grows in time. They checked that von Neumann's law[11] [$da_n/dt = K(n-6)$, where a_n is the area of an n-sided bubble] is a very robust description of the dynamics, even when the usual assumption of 120° angles at vertices fails.

Bubbles in monolayers look like a soap froth when the density in the liquid-gas coexistence region is near the gas border. Then the gas bubbles strongly pack, being separated by only thin liquid lines. Hence we call them "polygonal" bubbles. Previous experiments on stearic acid[12] and this study confirm the soap froth results, except that the growth exponent α (defined as $\langle a \rangle \sim t^{\alpha}$) is about 1.0 for monolayers instead of 0.6 for soap froths. As pointed out by Stavans and Glazier, this last value is probably due to three-dimensional effects[9] while $\alpha = 1$ is the value expected by dimensional analysis starting from von Neumann's law.[8,13]

In a different regime where the working density is in the central part of the coexistence plateau, the bubbles are circular and the liquid separation between them is of the order of their size. The bubbles are weakly interacting and advected by the motion of the liquid phase [of course we mean here the two-dimensional liquid phase and not the water subphase]. The dynamics of such "circular" bubbles is slower, with a growth exponent $\alpha \approx 0.6$. The most surprising result is that the tendency of the area distribution, at long times, follows a power law. Instead of reaching a scaling regime (i.e., a stable distribution when rescaled to a single time-dependent quantity like $\langle a \rangle$), the dynamics spontaneously introduces all length scales in the late-stage patterns, thus forming a critical object. Long-range dipolar interactions might be responsible for this phenomena (see Sec. IV).

The paper is organized as follows. In Sec. II we describe the experimental setup and present the observations. In Sec. III we analyze the data, and in Sec. IV we discuss the results.

II. THE EXPERIMENT

A. Setup and chemicals

To visualize the monolayer, we have used the fluorescence microscopy technique[14] developed recently. We in-

corporate some dye-labeled molecules in the film and look at their fluorescence. This method is extremely sensitive and powerful.[15] One observes good contrast between liquid and gas regions probably due to the large density difference. A criticism often raised about the fluorescence technique concerns the perturbation introduced by the dye impurities. In our case we need two coexisting isotropic fluid phases (here liquid and gas), and whether or not each one is a binary mixture of host molecules and dye impurities is irrelevant.

We used a 10-mW Ar^{3+} laser[16] (488 nm) to excite the fluorescence of the dye molecules. The laser beam reached the film by an oblique path without going through the microscope objective. The use of a laser enabled us to use a small amount of light, almost in the middle of the absorption band of the dye, achieving a very good luminosity with minimal temperature perturbation. We made the observations with a standard microscope, inserting a Schott OG515 filter in the light path to separate the fluorescence from the excitation light. For detection we used either a silicon intensified target (SIT) video camera,[17] or a sensitive photographic emulsion.[18] We used low magnification objectives (10× or 4×) in order to observe a large number of bubbles.

A small circular trough of fixed area $A = 0.71$ cm^2 was used to avoid large-scale motion of the monolayer. To study a film for a very long time (some remained intact for six days), we designed a closed cell. Figure 1 is a schematic cut of the cell. The bottom is a circular glass microscope coverslip. The body is made of Teflon with a platinum foil applied along the inner edge to achieve a hydrophilic wetting condition. To avoid meniscus effects, a teflon lip overhangs the platinum foil. This produces a well-defined and flat water surface (dashed line in Fig. 1). Another glass microscope coverslip closes the cell tightly, after the film has been spread in an argon atmosphere. The cell was made leakproof without glue by pressing the parts together in a lens holder. The whole cell was embedded in a temperature-controlled brass piece with an indium tin oxide (ITO) coated window to compensate for heat loss.

We used mainly two different chemicals: pentadecanoic acid with 1% of nitrobenzoxadiazole-hexadecylamine (NBD-HDA) as a dye and $L\alpha$-dipalmitoyl phosphotidylcholine (DPPC) with 1% $L\alpha$-phosphatidylcholine, β-NBD amino hexanoyl, γ-palmitoyl. All chemicals[19] were used as received. The subphase was ultrapure water ($\rho > 10$ MΩ cm) for the DPPC. In the case of pentadecanoic acid, we used a 10^{-2} mol dm^{-3} solution of hydrochloric acid to avoid dissociation of the acid molecule.

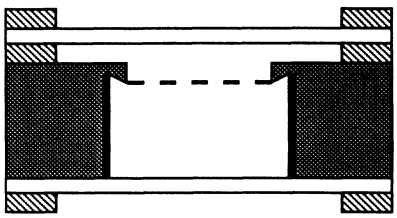

FIG. 1. Schematic cut of the cell. The water surface is indicated by a dashed line. The working surface is circular with area $=0.71$ cm^2. The cell is assembled in a lens holder (not shown here), which presses all the parts together. Hatched area, aluminum; solid area, platinum; dotted area, PTFE; open area, glass.

The monolayers were spread as follows: in an argon atmosphere, the clean trough was filled with a slight excess of water to produce a convex meniscus. We pumped carefully with a clean pipette to remove any contaminants or dust until we achieved a flat surface. We spread the monolayer with the solvent and let it evaporate for a few minutes in a large volume of argon. We then closed the cell and carried it from the glove box to the regulated environment on the microscope stage. We took as the origin of time the moment the film was spread.

Just after spreading, we observed, often but not always, a big homogeneous gas region in the center of the cell, a homogeneous liquid region in the exterior part, and in between gas bubbles in a liquid background, our region of interest. By controlling the amount of material spread, we were able to adjust the initial pattern from polygonal to circular bubbles. Finally, before describing the results, let us discuss some limitations of the experiment. At short times we are restricted by the evaporation of the solvent, which takes at least a few minutes. This is a very severe constraint. At long times observations are limited because the surfactant slowly escapes from the surface with a decay time of about one day for pentadecanoic acid and three days for DPPC. There are several possibilities for the leak: chemical dissociation of the molecules themselves, dissolution into the water subphase, or coating of the edges of the trough. More experiments are needed to solve this problem.

B. Experimental observations

For clarity, we mainly present two runs using pentadecanoic acid at the same temperature of 22.5 °C. We refer to them as run 1 and run 2. We started by spreading an amount of molecules such that the expected gas coverage (defined as the percentage of the total surface in the gas phase) was 89% for run 1 and 73% for run 2.[20] Of course the measured initial gas coverages were different (75% and 40%, respectively) because we only see a small region of the cell.

Figure 2 shows a time series of photographs taken from run 1. In the photos, the liquid phase appears bright and the gas phase dark. They were shot with 12500 ASA film using exposures from 5 to 15 sec. The resolution is about 3 μm and each image represents 2.27×3.30 mm^2. The run lasted about 3 h and the number of bubbles ranges from more than 1000 at the beginning to about 100 at the end. In Fig. 2(a), the majority of the bubbles are circular, although the big ones are deformed. In Fig. 2(b), most of the bubbles begin to deform by interaction with their neighbors. In time, the deformations increase, and at the end [Fig. 2(f)] only the smallest bubbles remain circular. Observing the dynamics of these geometrical networks is fascinating. We never saw any coalescence except at the end of the run, where the liquid lines between bubbles become so thin that they break. At this point, we stopped recording. The mecha-

nism of the coarsening occurred via a disappearance of small bubbles, in general three sided. Contrary to soap froths, we rarely saw four-sided and never five-sided bubbles disappear. On average, four-sided and five-sided bubbles shrunk, while seven-sided and more grew, as expected by von Neumann's law. Some bubbles changed their number of sides, either by the disappearance of a neighbor, or when a so-called T1 process occurred.[3] In a T1 process, two vertices are exchanged without changing the number of bubbles.

Figure 3 shows images from run 2, taken with a SIT video camera and averaged over 20 frames by computer. The image now corresponds to 0.90×1.19 mm^2. Note this run lasted 36 h, nearly an order of magnitude greater than run 1. Contrary to the preceding case, the bubbles remained circular for most of the time. Like the preceding case, the coarsening occurred without coalescence. A very characteristic scenario appears from these pictures: if one looks at the evolution of individual bubbles, one may notice that some which grow at a given time may shrink later. The critical size below which bubbles shrink and above which they grow, on average, is increasing with time. Consequently, there is no shortage of very small bubbles. In time, bigger and bigger bubbles move from expansion to contraction. One can see in Figs. 3(e) and 3(f) a dramatic illustration where the image is invaded by huge bubbles coming from outside the frame. All the bubbles from the starting image, even the ones which have grown, may eventually disappear to leave room to these giants.

Figures 3(e) and 3(f) show a striking feature that we have observed on at least two runs. Secondary nucleation of tiny liquid droplets in the gas bubbles was seen at about $t \sim 500$ min. There were several of these spots in each gas bubble. Their size was about 5 μm at most and their Brownian motion was visible. They appeared after a significant coarsening of the system, but did not seem to affect the growth. We never observed this phenomenon

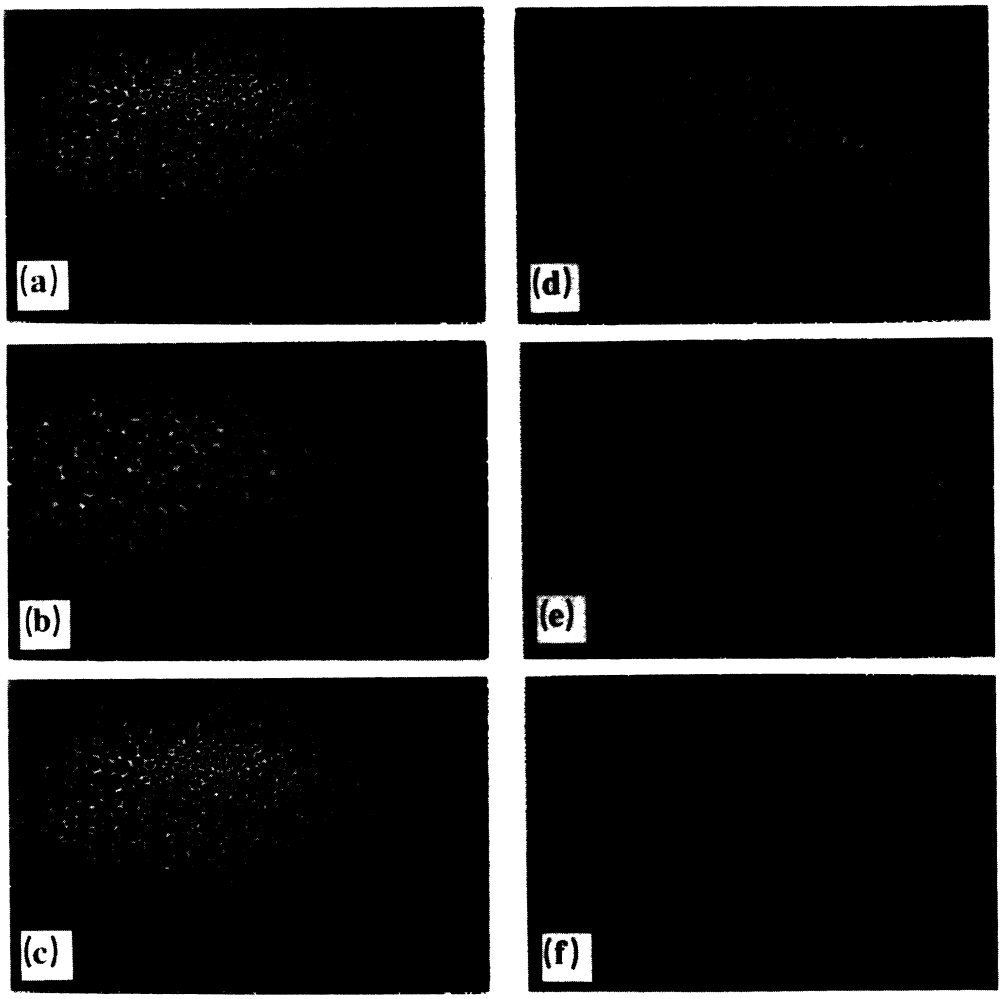

FIG. 2. Time series from run 1. One sees photographs (shot with 12500 ASA Kodak film) obtained by fluorescence microscopy of pentadecanoic acid with 1% of dye molecule (see text), at $T = 22.5$ °C. The gas bubbles are dark and the liquid phase appears bright. The measured initial gas coverage is 75%. The shots (a)–(f) were taken at $t = 6$, 23.5, 38.5, 67.5, 103, and 147 min, respectively, after spreading. The size of each individual frame is 2.27×3.30 mm^2.

with polygonal bubbles; for instance, they did not appear in run 1 (see Sec. IV).

III. STATISTICAL ANALYSIS

A. Area

Figure 4 shows the mean area as a function of time for run 1 (squares) and run 2 (circles) in a log-log plot. We calculated the mean area by dividing the total gas surface in a picture by the total number of bubbles, including those cut by the border if more than one half of the bubble was inside. This method is better than suppressing every border bubble when big bubbles invade the frame, as in Fig. 3(e) or 3(f). Figure 4 shows that for each run there are three regimes. The first one is a transient lasting several minutes. It is followed by a slow growth regime where the mean area follows a power law, with $\alpha \approx 0.6$. Finally a fast growth regime appears where $\alpha \approx 1.0$. The crossover between these regimes occurs at about $t = 70$ min for run 1 and $t = 400$ min for run 2. This crossover corresponds to the point where bubbles change from circular to polygonal for run 2, but does not quite coincide for run 1. Nevertheless, there is no reason to expect an exact coincidence. With confidence we can say that polygonal bubbles evolve with a growth exponent $\alpha \approx 1.0$ and circular bubbles with $\alpha \approx 0.6$. Notice that run 1 starts with much bigger bubbles than run 2. We observed this as a systematic trend, i.e., the more polygonal the initial configuration, the bigger the bubbles and the faster they evolve. As discussed in Sec. IV, this may be a signature of dipolar interactions.

Figures 5(a) and 5(b) show the evolution of the second moment of the area distribution, defined as

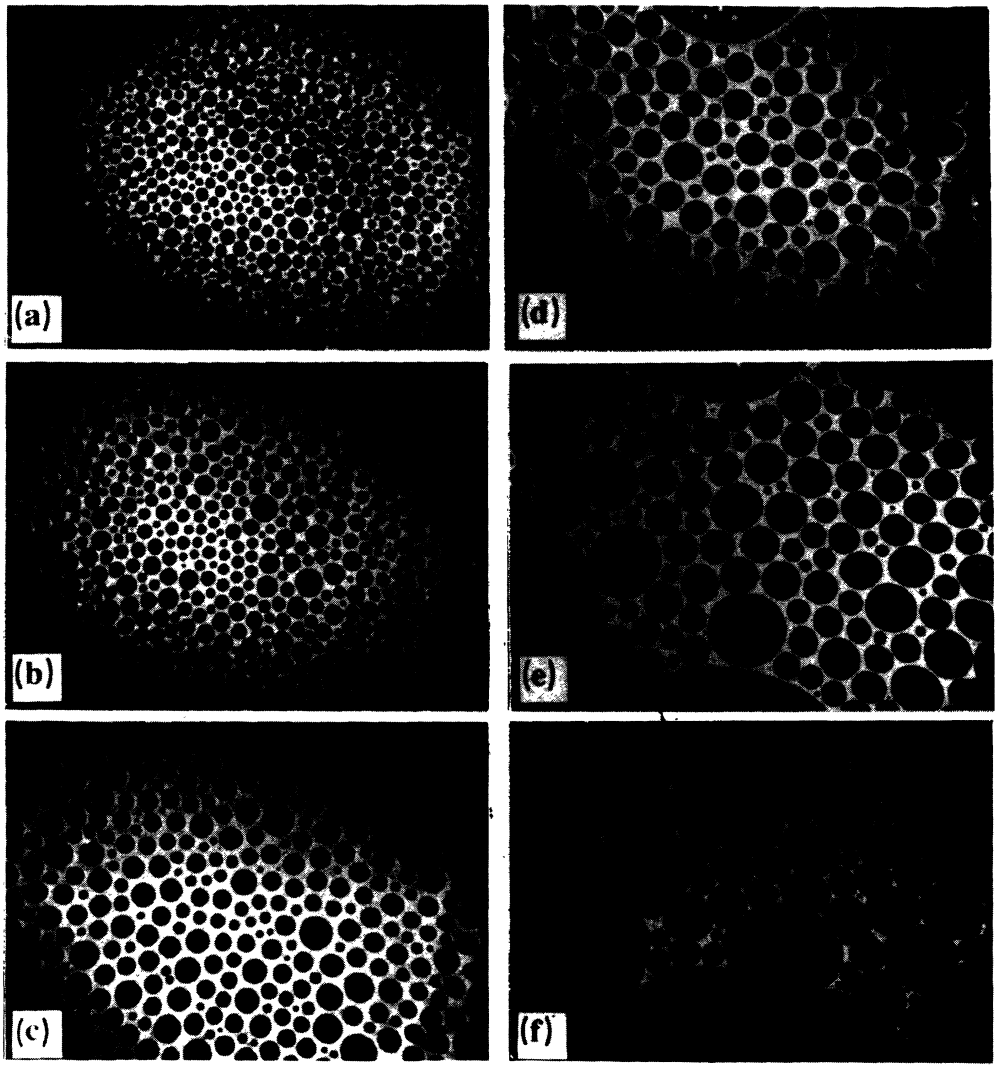

FIG. 3. Time series from run 2. The conditions are the same as in Fig. 2, but with an initial gas coverage of 40%. The images are the result of numerically averaging 20 frames taken from a SIT video camera. The images (a)–(f) were taken at $t = 9$, 20.5, 83, 319, 681, 1469 min respectively. The size of each individual frame is 0.90×1.19 mm^2.

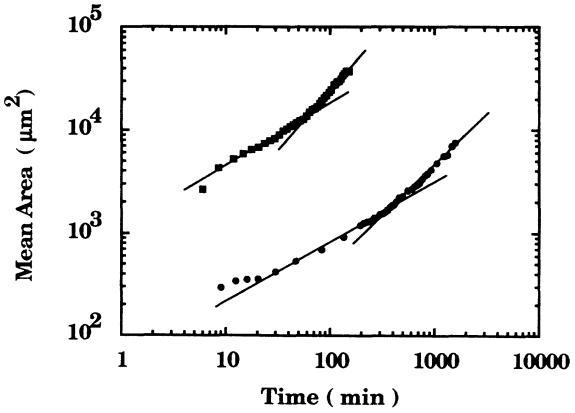

FIG. 4. Mean area as a function of time, for run 1 (squares) and run 2 (circles), in a log-log plot. The straight lines indicate the different power-law regimes (see text).

$$\lambda_2=\frac{\langle a^2\rangle-\langle a\rangle^2}{\langle a\rangle^2}\ , \tag{1}$$

for run 1 and run 2, respectively. For run 1, this quantity reaches rapidly an asymptotic value of 0.5. This is the expected behavior for a scaling regime where all the higher moments of the area distribution, once rescaled to the first one $\langle a\rangle$, should be constant. On the contrary, in run 2 the second moment of the distribution increases continuously, as shown in Fig. 5(b). This indicates that

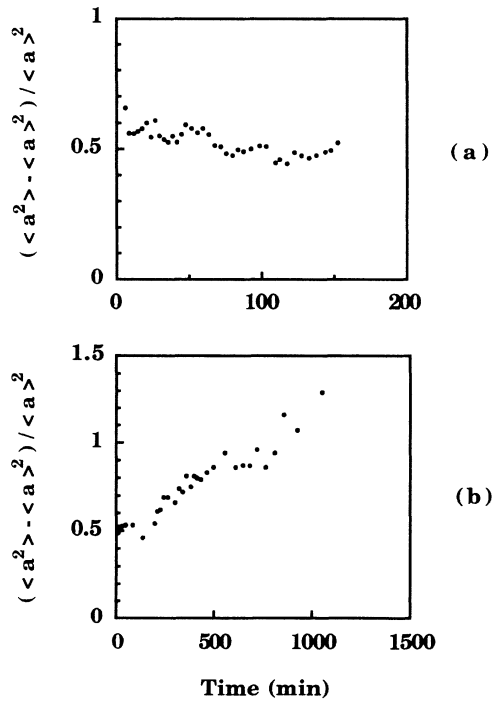

FIG. 5. Second moment of area distribution as a function of time, (a) for run 1 and (b) for run 2. Note that the second moment is defined as a dimensionless quantity.

the shape of the distribution does not reach a stable form, but broadens continuously. It is thus interesting to look at the distribution functions themselves.

Figure 6 shows the probability distribution for bubble areas at three different times for run 1 (a)–(c) and run 2 (d)–(f), in log-log plots. The area distribution was computed using a coarse graining procedure, averaging over four bins of the area histograms. As shown in Figs. 6(a) and 6(d), both runs start from quite similar area distributions. There is a lower bound due to the finite resolution. The distribution seems to be flat with an upper cutoff. Nevertheless, in time, one observes different behaviors. For run 1, both the lower and the upper cutoff shift to larger areas. For instance, in Fig. 6(c), there are no bubbles smaller than 2000 μm^2 and we have drawn a line to indicate that the probability distribution should be very small in this region. Thus run 1 ends up with a peaked distribution. Indeed, we have not verified the scaling hypothesis, i.e., that the shape does not change once properly rescaled. Nonetheless, the measured distributions are compatible, and the behavior of the second moment [see Fig. 5(a)] strongly suggests the hypothesis. For run 2, only the upper cutoff is shifted to larger areas, not the lower one. Hence, even at the end of the run, one still finds tiny bubbles. At intermediate times [Fig. 6(e)], the distribution looks like a broad peak superimposed on a smoothly decreasing base line. At the end [Fig. 6(f)], one no longer sees a peak but only a decreasing curve, described by a power law:

$$P(a)\sim a^{-\nu}\ , \tag{2}$$

with $\nu=0.6$ and an upper cutoff at about 5000 μm^2.

This behavior was observed in at least two runs done under the same conditions with pentadecanoic acid, and also in a long run (48 h) done with DPPC, starting from slightly smaller bubbles and the same gas coverage ($\sim$45%). Figure 7(a) shows the area distribution measured from Fig. 7(b) at the end of the DPPC run. One sees a power law with an exponent $\nu\approx 1.0$ over two and a half decades. Figure 7(b) illustrates the fractal character of the object with details on all length scales. Two of the big bubbles in Fig. 7(b) contain liquid droplets. These droplets, which were present from the beginning of the run, were discarded when computing the area distributions.

B. Number of sides

Figure 8 shows the number of sides probability distribution, measured during run 1, at three different times. To compare with soap froths, we have computed the second moment of the number of sides distribution, as defined in Ref. 9:

$$\mu_2=\langle n^2\rangle-\langle n\rangle^2\ , \tag{3}$$

and found that it fluctuates around a value of the order of $\mu_2\sim 1.4$. Within experimental error, this value is close to the one observed by Stavans and Glazier in soap froths, which shows that the topology is similar in both cases. It is possible that this number follows directly from von Neumann's law.

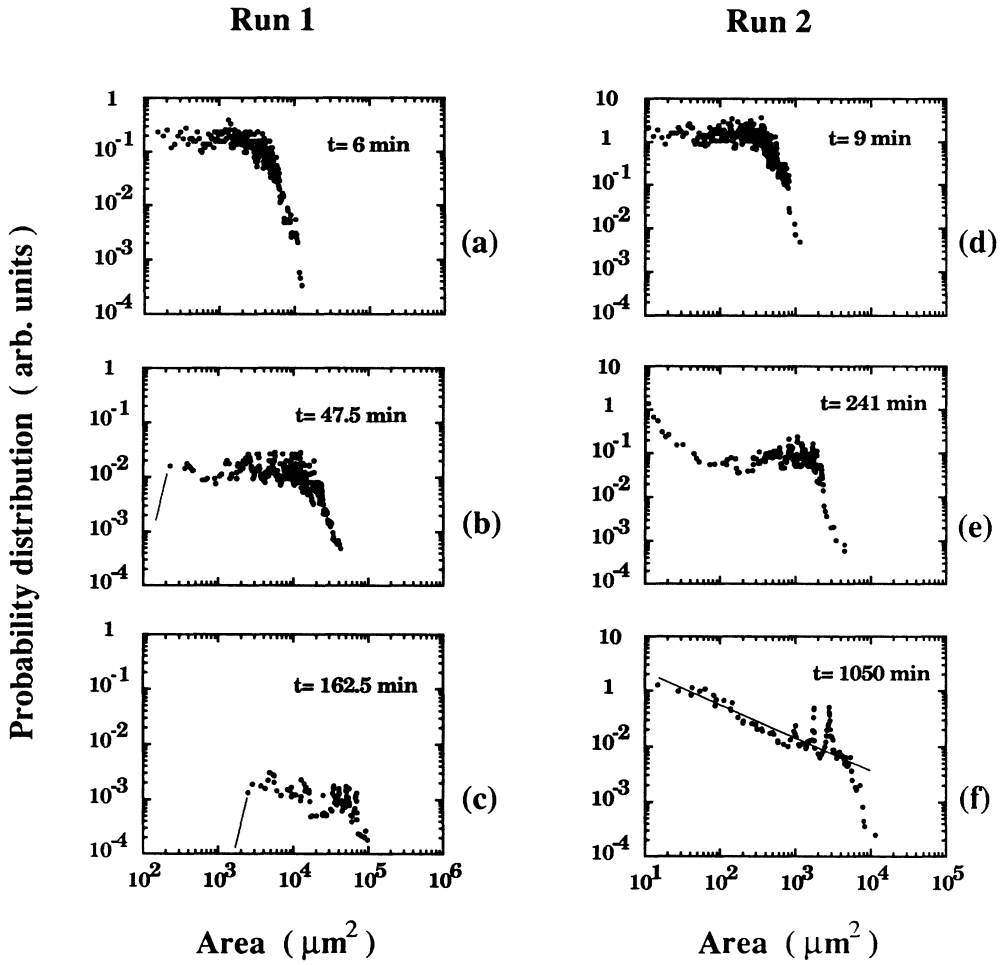

FIG. 6. Area probability distribution for run 1 [(a) $t=6$ min, (b) $t=47.5$ min, (c) $t=162.5$ min] and run 2 (d) $t=9$ min, (e) $t=241$ min, (f) $t=1050$ min], in log-log plots (see text). The lines in (b) and (c) indicate the tendency of the distribution. In (f), the added line indicates the power-law nature of the distribution and has a slope of 0.6.

C. Repulsion between bubbles

Using run 1, where the bubbles are clearly deformed, we analyzed the repulsion between bubbles. Their shape is the result of the competition between line tension, which favors a circular shape, and repulsion from neighbors, which would lead to polygonal bubbles. For a given bubble, we measured the border's curvature at closest interaction with a neighbor and compared it to its curvature far from other bubbles (e.g., at vertices). Assuming constant pressures inside a bubble and in the nearby liquid, one can balance forces on an element of interface and deduce the repulsion between bubbles. This analysis proceeds only from geometrical considerations, thus we calculate the force in terms of the interfacial line tension λ, which remains an unknown parameter. Figure 9 shows the repulsion force per unit length of interface divided by λ as a function of the liquid thickness between bubbles. The curve is stable in time but should be regarded only as indicative.

IV. DISCUSSION

In this section we would like to compare our observations with classical theories and then investigate the role of dipolar interactions. In the "circular" bubble regime, the mean area grows with an exponent close to the one found for Ostwald ripening,[21,22] $\alpha=\frac{2}{3}$. Nevertheless, all the theories predicting such an exponent assume an asymptotic scaling regime, which is found in numerical simulations.[23] But our results clearly rule out this assumption. We are thus left with an open problem.

Now, let us address the following question: Why are runs 1 and 2, which differ only in initial gas coverage, so different? It is known for soap froths that any perturbation extends only to nearest neighbors.[9] This is also true for run 1 due to the strong bubble packing. Our first thought was that in run 2 there is more space between bubbles and the correlations might extend much farther. In Ostwald ripening in two dimensions, Marqusee[22] has pointed out that the mutual influence of two bubbles is

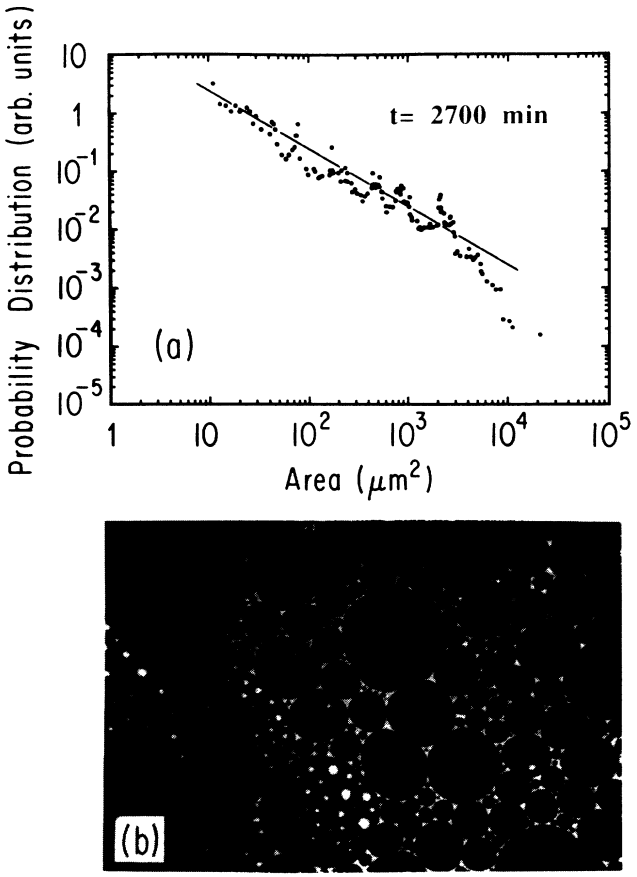

FIG. 7. (a) Probability distribution for areas, at the end of a run done with DPPC ($t=2700$ min), in a log-lot plot. The straight line has a slope of 1.0. (b) The corresponding image, obtained with the SIT video camera. The small liquid droplets seen in two of the gas bubbles were present from the start and do not contribute to the area probability distribution.

screened by the effective medium formed by all the others. For a gas coverage of 40%, he calculated a screening length of the order of the nearest-neighbor distance. This indicates that in both runs, the screening is short ranged

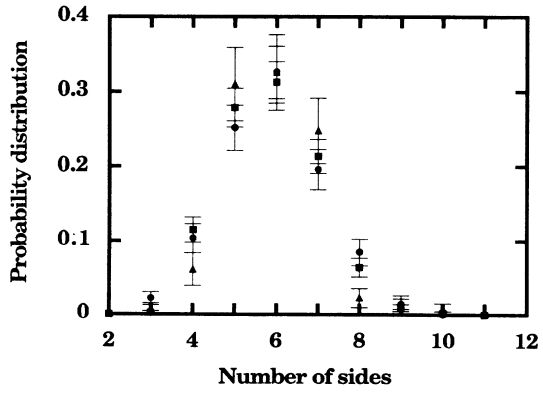

FIG. 8. Probability distribution for the number of sides at three different times (squares at $t=17.5$ min, circles at $t=71.5$ min, triangles at $t=137.5$ min) for run 1.

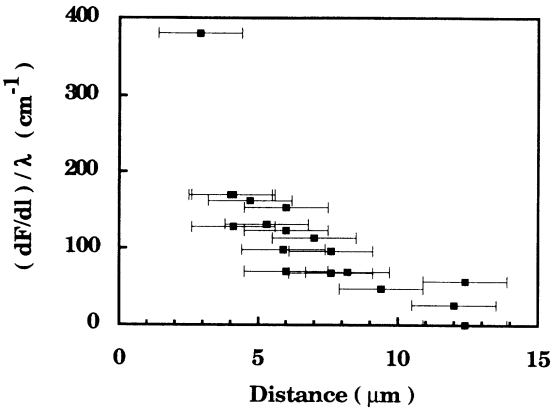

FIG. 9. Repulsion between two bubbles vs separation. We have plotted the repulsion force per unit length of interface, divided by its line tension λ as a function of distance between bubbles.

and cannot account for the difference of their evolutions.

Let us now investigate the role of long-range interactions between molecular electric dipoles moments, which we believe are responsible for the difference. For monolayers, Andelman *et al.*[24] have shown that the screening by the water subphase is incomplete, so that the dipolar interaction is weaker but remains long ranged. For liquid-gas domains at equilibrium, they calculated that the amplitude of the dipolar interactions is maximal in the middle of the coexistence plateau and vanishes at its ends.[25] From this result and the stated gas coverages, one expects the dipolar interactions to be much stronger in run 2 than in run 1. These interactions should be even stronger for the DPPC run, because this molecule has a larger electric dipole moment and the electrostatic screening by the subphase was weaker (recall for DPPC we used pure water). Hence we believe that the strength of the long-range dipolar interactions between bubbles is responsible for the presence of a critical pattern in run 2 and in the DPPC run (see Fig. 7). In the case of monolayers, it is not clear whether the dipolar field of one bubble is screened by the others, or not.

In addition, dipolar effects could account for two other experimental observations. First, bubbles created in the initial configuration are systematically larger near the gas boundary than in the middle of the coexistence plateau (e.g., run 1 versus run 2). We can understand this if initially the typical bubble size scales like the optimal periodicity D, introduced by Andelman *et al.* for parallel alternating liquid and gas stripes. This periodicity D is the result of a balance between dipolar and interfacial energies, and is expected to diverge at the boundaries of the plateau region.[24] Second, we observed nucleation of small liquid droplets in the gas bubbles at late stages. If initially the typical bubble size compares with the preferred periodicity D, then after coarsening, the two lengths will no longer match. Hence, this secondary nucleation could be a means to reintroduce high spatial frequencies.

V. CONCLUSIONS

This paper presents an experimental study of the evolution of gas bubbles in lipid monolayers. We studied mainly two different regimes. In the first one, the gas phase is predominant and thin liquid lines separate the polygonal bubbles. This pattern coarsens like a two-dimensional soap froth, except that the growth exponent $\alpha \approx 1.0$ is the result obtained by dimensional analysis. This confirms von Neumann's law as a good mean-field description for these systems.

The other regime, circular bubbles, appears for gas coverage of about 50%. Here, the liquid separation between gas bubbles is of the order of their size. The growth is slower with an exponent $\alpha \approx 0.6$. We observe that the pattern, instead of reaching a scaling state, evolves spontaneously toward a critical state. The area distribution probability follows a power law $P(a) \sim a^{-\nu}$. Whether or not the exponent ν is material dependent is an open question, since we observed a value of 0.6 for pentadecanoic acid and 1.0 for DPPC. We show that the strength of the dipolar interactions is the likely parameter responsible for the evolution to a critical pattern.

ACKNOWLEDGMENTS

We would like to thank James Glazier for his help in defining the goals of this experiment. We have appreciated many discussions with Marcelo Magnasco, who had stimulating ideas about the interplay of growth and advection in bubble arrays. We are also indebted to Elisha Moses and Pierre Molho for many fruitful discussions and concrete help in software. Finally, we thank Thomas Witten, who pointed our attention to dipolar effects. One of us (B.B.) received financial support from a joint program Centre National de la Recherche Scientifique (France)-National Science Foundation (NSF) (USA). This work was supported by the NSF under Grant No. DMR-8722714.

---

*Permanent address: Laboratoire de Spectrométrie Physique, Domaine Universitaire, 38402 St. Martin d'Hères, France.

[1]A. Miller, W. Knoll, and H. Möhwald, Phys. Rev. Lett. **56**, 2633 (1986).

[2]R. M. Weis and H. M. McConnell, Nature **310**, 47 (1984); W. M. Heckl and H. Möhwald, Ber. Bunsenges. Phys. Chem. **90**, 1159 (1986).

[3]D. Weaire and N. Rivier, Contemp. Phys. **25**, 59 (1984).

[4]A. Brin and R. Merigoux, C. R. Acad. Sci. (Paris) **238**, 1808 (1954); C. M. Knobler and D. Beysens, Europhys. Lett. **6**, 707 (1988).

[5]K. L. Babcock and R. M. Westervelt, Phys. Rev. A **40**, 2022 (1989) and references therein.

[6]Darcy Thompson, *On Growth and Form*, 2nd ed. (Cambridge University Press, Cambridge, England, 1942).

[7]J. D. Gunton, M. San Miguel, and P. Sahni, *Phase Transitions and Critical Phenomena*, edited by C. Domb and J. L. Lebovitz (Academic, London, 1983), Vol. 8, p. 267.

[8]J. A. Glazier, S. P. Gross, and J. Stavans, Phys. Rev. A **36**, 306 (1987).

[9]J. Stavans and J. A. Glazier, Phys. Rev. Lett. **62**, 1318 (1989).

[10]J. A. Glazier, Ph.D. thesis, the University of Chicago, 1989 (unpublished).

[11]J. von Neumann, in *Metal Interfaces*, edited by C. Herring (American Society for Metals, Cleveland, OH, 1952), p. 108.

[12]B. Moore, C. M. Knobler, D. Broseta and F. Rondelez, J. Chem. Soc. Faraday Trans. II **82**, 1753 (1986).

[13]M. Marder, Phys. Rev. A **36**, 438 (1987).

[14]M. Lösche, E. Sackmann, and H. Möhwald, Ber. Bunsenges. Phys. Chem. **87**, 848 (1983); R. Peters and K. Beck, Proc. Natl. Acad. Sci. USA **80**, 7183 (1983); H. M. McConnell, L. K. Tamm, and R. M. Weis, *ibid.* **81**, 3249 (1984).

[15]A. Fisher, M. Lösche, H. Möhwald, and E. Sackmann, J. Phys. Lett. **45**, L-785 (1984).

[16]Model No. 161-C, Spectra-Physics, Mountain View, CA.

[17]Model No. 5000, COHU, San Diego, CA.

[18]3200 ASA Kodak Tmax, pushed to 12500 ASA.

[19]Both the pentadecanoic acid (Aldrich Chemical Co., No. P360-0) and $L\alpha$-DPPC (Sigma Chemical Co., No. P-6267) were quoted as 99+% pure. The NBD-Hexadecylamine (Molecular Probes Inc., Eugene, OR 97402, No. H-429) was suggested by F. Rondelez. The hydrophillic part of the dye molecule is the NBD group itself. The $L\alpha$-phosphatidylcholine, β-NBD amino hexanoyl, γ-palmitoyl (Sigma Chemical Co., No. P-3412) was quoted as 98% pure.

[20]The density of the liquid and gas phases at this temperature are taken from N. R. Pallas and B. A. Pethica, J. Chem. Soc. Faraday Trans. I **83**, 585 (1987).

[21]I. M. Lifshitz and V. V. Slyosov, Phys. Chem. Solids **19**, 35 (1961); K. Binder, Phys. Rev. B **15**, 4425 (1977).

[22]J. A. Marqusee, J. Chem. Phys. **81**, 976 (1984).

[23]T. M. Rogers and R. C. Desai, Phys. Rev. B **39**, 11 956 (1989); J. G. Amar, F. E. Sullivan, and R. D. Mountain, *ibid.* **37**, 196 (1988).

[24]D. Andelman, F. Brochard, and J.-F. Joanny, J. Chem. Phys. **86**, 3673 (1987).

[25]See Eq. 32 of Ref. 24.

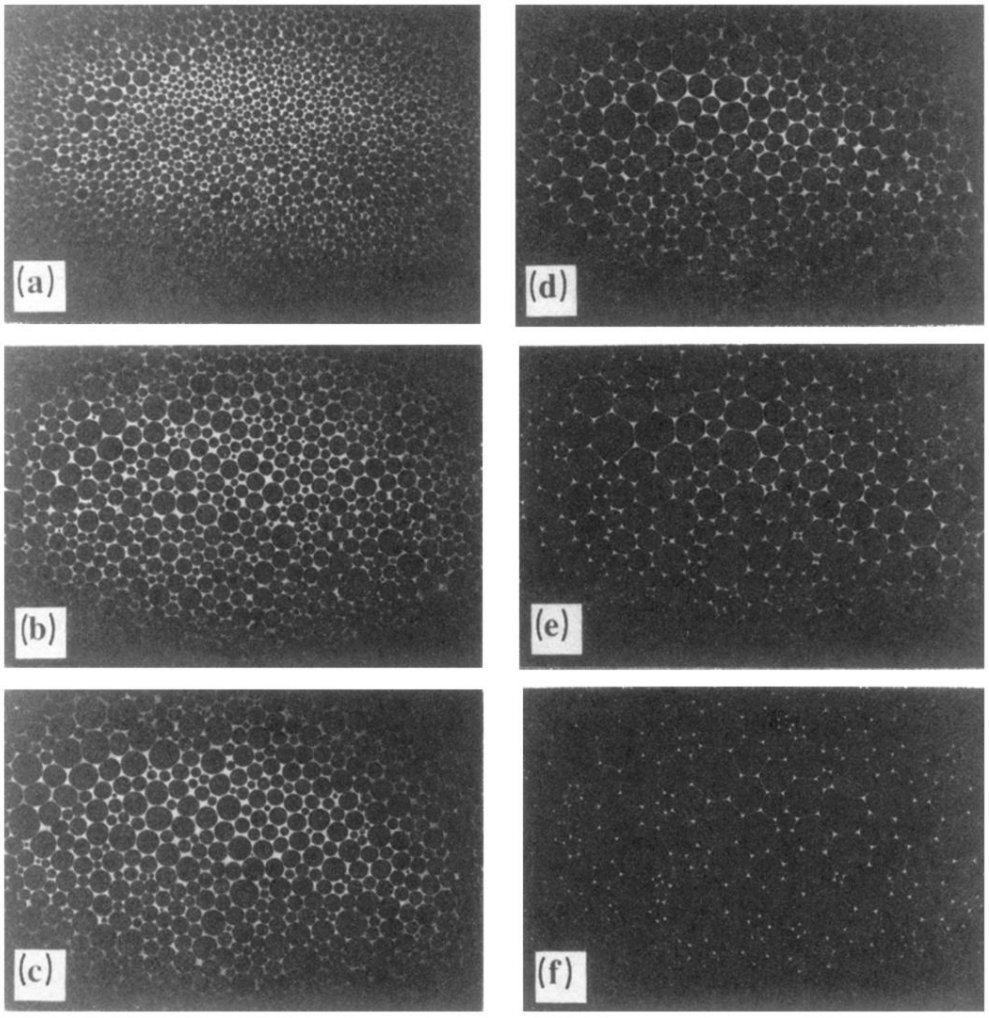

FIG. 2. Time series from run 1. One sees photographs (shot with 12500 ASA Kodak film) obtained by fluorescence microscopy of pentadecanoic acid with 1% of dye molecule (see text), at $T = 22.5\,^{\circ}\mathrm{C}$. The gas bubbles are dark and the liquid phase appears bright. The measured initial gas coverage is 75%. The shots (a)–(f) were taken at $t = 6$, 23.5, 38.5, 67.5, 103, and 147 min, respectively, after spreading. The size of each individual frame is $2.27 \times 3.30\ \mathrm{mm}^2$.

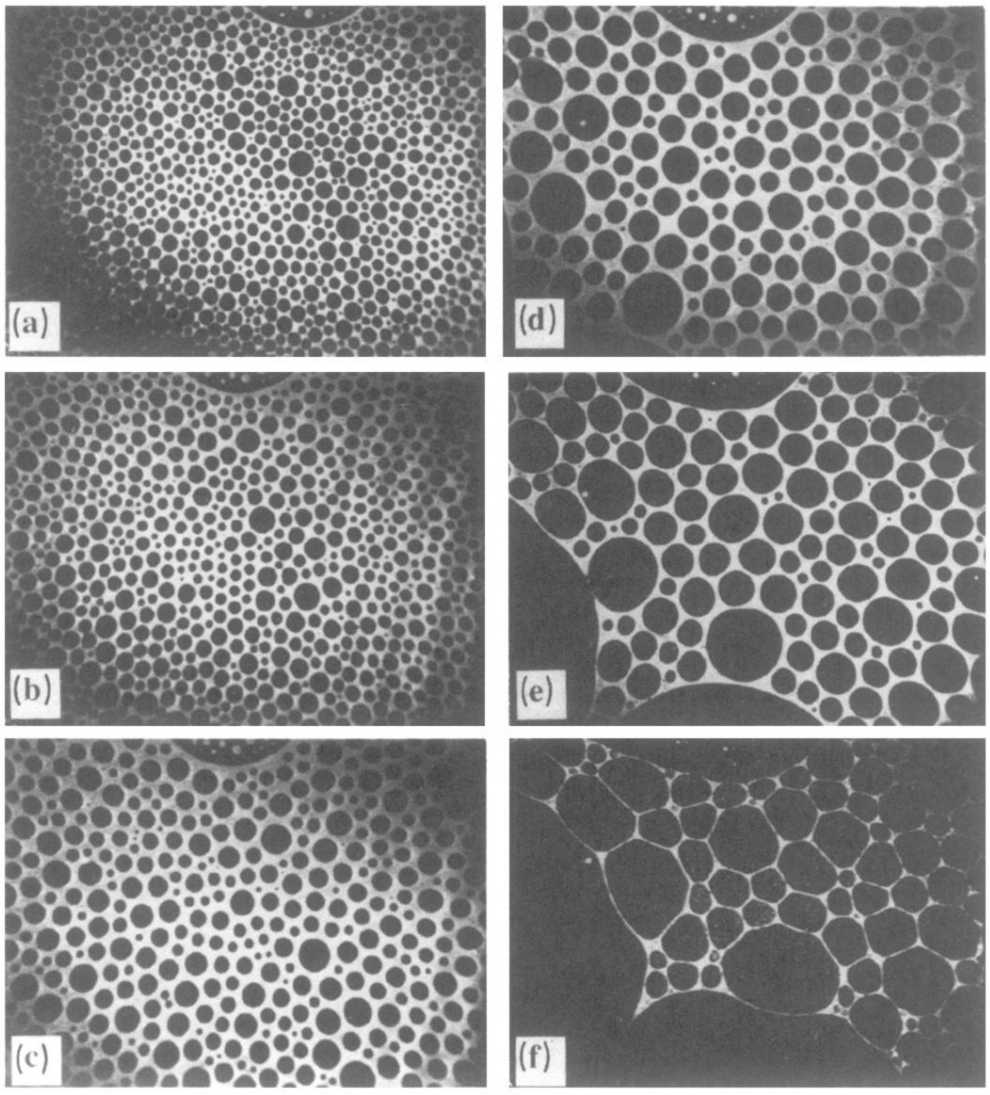

FIG. 3. Time series from run 2. The conditions are the same as in Fig. 2, but with an initial gas coverage of 40%. The images are the result of numerically averaging 20 frames taken from a SIT video camera. The images (a)–(f) were taken at $t = 9$, 20.5, 83, 319, 681, 1469 min respectively. The size of each individual frame is 0.90×1.19 mm^2.

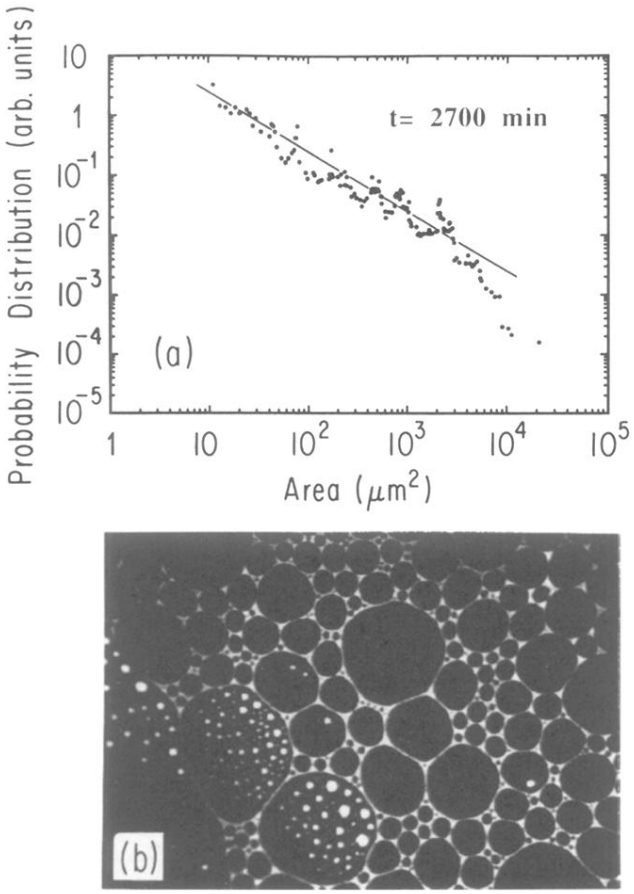

FIG. 7. (a) Probability distribution for areas, at the end of a run done with DPPC ($t = 2700$ min), in a log-lot plot. The straight line has a slope of 1.0. (b) The corresponding image, obtained with the SIT video camera. The small liquid droplets seen in two of the gas bubbles were present from the start and do not contribute to the area probability distribution.